

characteristics, have been demonstrated for neuromorphic computing architectures.

In this work, we demonstrate an optical memory consisting of a VO₂ microwire integrated on a Si photonic waveguide (Figure 1). The memory exploits the inherent bistable

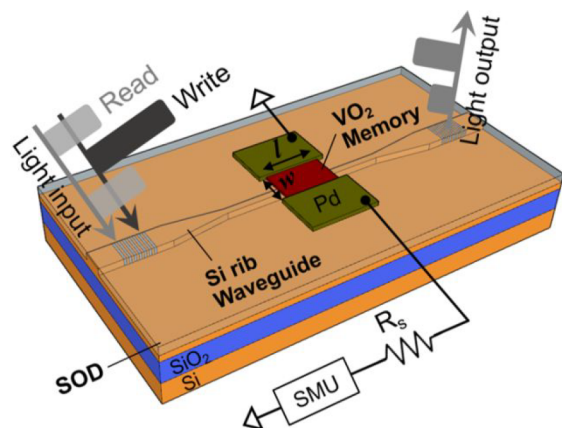


Figure 1. Schematic of the waveguide-integrated VO₂-Si optical memory. SOD stands for “spin-on dielectric”, and SMU stands for “source measure unit”.

characteristics of the hysteresis across the IMT in VO₂. An optical pulse is used to write the VO₂ memory cell integrated atop the waveguide, and the memory (written or not written) is stored as the material state of VO₂ (metal or insulator). The written memory is read out as a change in the optical transmission and the electrical current caused by the state of VO₂. Both the read and write light signals are delivered by an integrated optical waveguide, enabling on-chip integration. In contrast to GST optical memories, our device does not require

specially tailored pulse shapes or trains for writing or erasing. The ON/OFF contrast and optical writing energy are investigated as a function of device length.

DEVICE CONCEPT

Figure 1 shows a schematic of the hybrid VO₂-Si waveguide structure and the optical memory operation. A VO₂ wire with two electrical terminals is controlled by an incident optical signal. When the device is biased with a voltage, the IMT is induced by thermal- and field-induced carrier generation and a hysteresis is usually observed (Figure 3a).²⁸ This hysteretic behavior leads to the nonlinear current–voltage (*I*–*V*) characteristic and the switched state to be maintained, which can be utilized for memory.

To investigate the device for optical memory, we used the combination of an optical writing pulse and a voltage bias. The device is first held at a constant voltage bias within the IMT hysteresis and then a light pulse at a wavelength of 1.5 μm in our experiment is launched through a grating coupler to write the VO₂ memory. Both writing and reading of the memory leverage the interaction between the evanescent field of the guided optical mode and the VO₂ on top of the Si waveguide. The excess carrier generation induced by photocarrier doping and photothermal effects triggers the Mott-assisted Peierls structural phase transition (SPT) to the metal state.^{13,20} Even after the light pulse is removed, the device remains in the written metal state under the voltage bias. Reducing the applied voltage to zero resets the VO₂ to its original insulator state. The phase of the VO₂ affects the optical transmission of the underlying waveguide, so the memory can be read optically by monitoring the waveguide output transmission. The memory can also be read out as a change in the current (and/or resistance) of the device at the bias terminals.

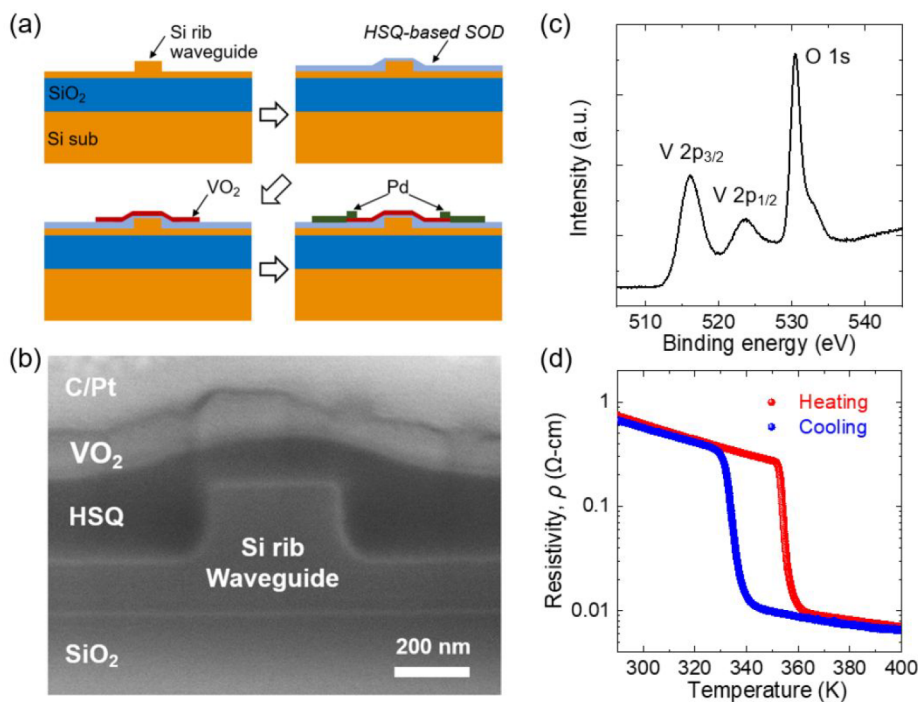


Figure 2. Device preparation and material characterization. (a) Device fabrication process. (b) Cross-sectional SEM image of a representative device with VO₂ deposited on the Si waveguide after planarization using HSQ. (c) XPS spectrum of a VO₂ film. (d) Resistivity of a VO₂ device as a function of the stage temperature (red dots: heating; blue dots: cooling).

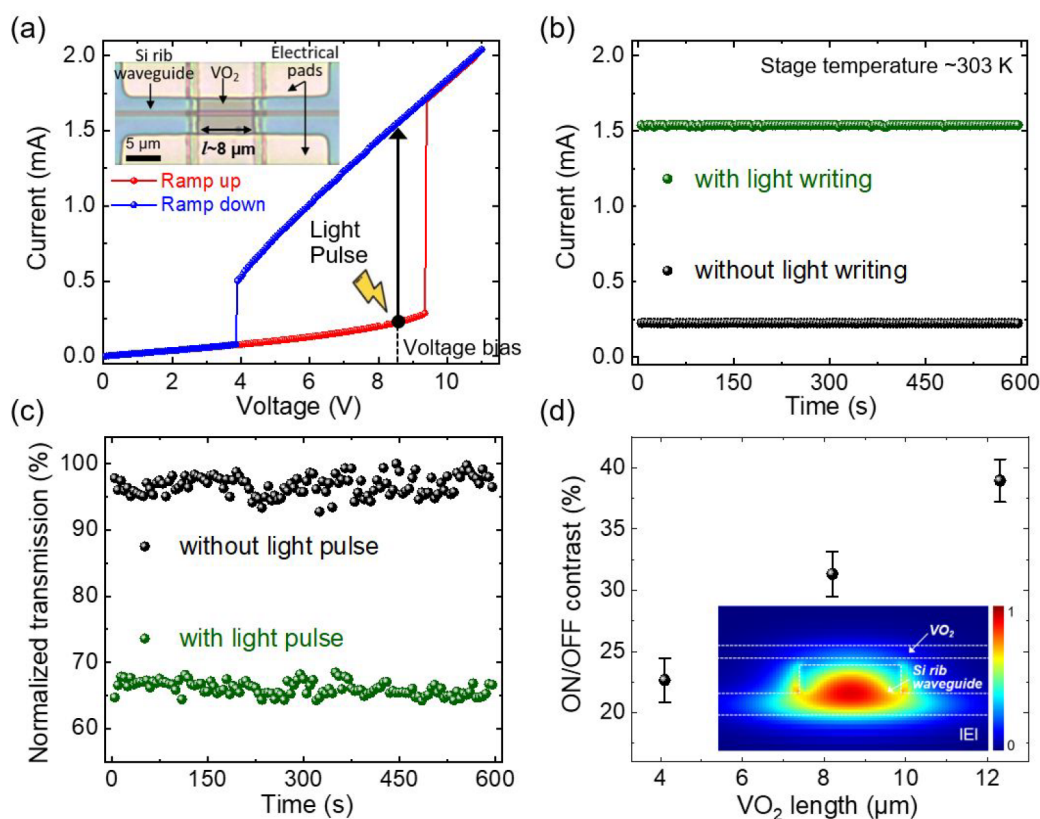


Figure 3. Operation of a voltage-biased VO₂ optical memory device. (a) I – V measurement at a temperature of ~ 303 K (Red dotted line: voltage ramp up, blue dotted line: voltage ramp down), showing the IMT hysteresis. For the optical memory writing, a ~ 150 ms-long optical pulse at an optical power of ~ 820 μ W was incident on the VO₂ biased at 8.5 V. The laser wavelength was 1.5 μ m. The inset shows the top view of the measured device. Time trace of (b) DC current and (c) normalized optical transmission readout after turning off the laser pulse. (d) ON/OFF contrast as a function of the VO₂ length. The inset shows the magnitude of the electric field ($|E|$) of the optical mode (TE polarized).

■ DEVICE FABRICATION AND MATERIAL CHARACTERIZATION

Figure 2a shows device fabrication process. Si rib waveguides with a thickness of ~ 400 nm, an etch depth of ~ 250 nm, and a width of ~ 450 nm for single-mode waveguiding at a wavelength of 1.5 μ m were fabricated through standard electron beam (e-beam) lithography and inductively coupled plasma reactive ion etching. Surface grating couplers at the end of the waveguides were placed for fiber-to-waveguide light input/output coupling. Next, a flowable hydrogen silsesquioxane (HSQ)-based spin-on-dielectric (SOD) was applied to make a flat top for the formation of the VO₂ strip atop the Si waveguide. The main advantage of using HSQ was that no cracks were formed during fabrication processes carried out at high temperatures of >600 °C (e.g., thermal curing and VO₂ growth). The chip was spin-coated at a speed of 2000 rotations per minute (rpm) with HSQ (XR-1541 6%), followed by thermal curing at a temperature of 600 °C for 30 min to dissociate Si–H bonds to form SiO₂.²⁹ A polycrystalline VO₂ film with a thickness of ~ 100 nm was deposited on top by pulsed laser deposition. The VO₂ target was irradiated by focused pulses from a 248 nm KrF excimer laser at a growth temperature of 530 °C under oxygen partial pressure of 9.5 mTorr. The VO₂ film was wet-etched into a wire shape using a chromium (Cr) etchant. The wire length (l) varied from 4 to 12 μ m, and the wire width (w) was fixed at ~ 5 μ m. The metal (palladium, Pd) contact pads were formed atop the VO₂ wire

using typical photolithography, e-beam evaporation deposition, and lift-off steps.

Figure 2b shows a cross-sectional scanning electron micrograph (SEM) of a fully processed hybrid VO₂–Si waveguide device, highlighting the details of the continuous VO₂ film as well as the optical coupling region between the VO₂ wire and the Si rib waveguide. The elemental composition and valence state were measured by X-ray photoelectron spectroscopy (XPS), as shown in Figure 2c. The surface was gently cleaned by cluster ion etching prior to the measurement. The two strong peaks at 516.1 and 523.7 eV correspond to V 2p_{3/2} and V 2p_{1/2}, respectively, which can be assigned to the characteristic of the V⁴⁺ oxidation state.³⁰ The measured resistivity of the VO₂ film as a function of stage temperature (Figure 2d) displays the transitions at ~ 355 and ~ 335 K during heating and cooling cycles for IMT and metal–insulator transition (MIT), respectively. Across the phase transition, the VO₂ resistivity changed by about 2 orders of magnitude.

■ RESULTS AND DISCUSSION

For the electrical characterization, we ramped the voltage up and down between 0 and 11 V in 50 mV increments with an external resistor ($R_s = 5$ k Ω) connected in series. All measurements were conducted at a temperature of ~ 303 K. The integrated VO₂ wire had a width of 5 μ m, and the optical propagation length in the hybrid VO₂–Si waveguide section, l , was about 8 μ m (inset of Figure 3a). The IMT occurred around 9.35 V with the complete SPT, which resulted in a

sharp increase in the current, as shown in Figure 3a. During the ramp down (blue dotted line), the reverse MIT did not occur at the same voltage as the ramp up. The VO₂ device exhibited a hysteresis with bistable states, which we utilized for the optical memory.

The operation of the optical memory was as follows: A voltage bias was applied to bring the VO₂ within the IMT hysteresis loop such that a light pulse induced the VO₂ into the metal state. Since the IMT was at ~ 9.35 V, we applied a voltage bias of ~ 8.5 V (denoted by black dotted line in Figure 3a) and then turned on a ~ 150 ms-long laser pulse to write the memory state. The laser pulse with a wavelength of $1.5 \mu\text{m}$ was first injected from an optical fiber into the Si waveguide through the grating coupler, and light propagating along the waveguide was coupled into the VO₂ evanescently. When biasing the device at ~ 8.5 V, a minimum optical writing power of about $490 \mu\text{W}$ in the waveguide was required. In the experiments to follow, an incident optical power of about $820 \mu\text{W}$ was used for reliable writing of the VO₂. The measured insertion loss from the VO₂ wire was $\sim 0.95 \text{ dB}/\mu\text{m}$. Figure 3b plots the first 10 min of the device current reading with (green) and without (black) an incident laser pulse. Even after the laser was turned off, the current readout of the device did not return to its original insulator-state current, and the VO₂ was latched in the metal state with a measured DC current of ~ 1.55 mA while maintaining the voltage bias.

The VO₂ state was also read out optically using a ~ 1 s long laser pulse with a wavelength of $1.51 \mu\text{m}$ and at least $5\times$ less power than the write pulse. The optical absorption depended on phase of the VO₂, so the memory state could be read out by the optical transmission in the waveguide. Because metallic state of VO₂ attenuated the optical transmission relative to the insulator state, the normalized optical transmission was reduced to $\sim 66\%$ (green dots in Figure 3c). The black dots in Figure 3b,c show that when the writing optical pulse was not applied, the device remained in the insulator state with low current readout (~ 0.2 mA) and high optical transmission ($\sim 98\%$). The device retained the written memory state for at least 200 h if the voltage bias was maintained.

Figure 3d plots the ON/OFF contrast of the memory state with respect to the VO₂ length. The ON/OFF contrast is defined as the optical transmission difference between initial insulator and written metal state. The average and standard deviation was obtained from 100 measurements for each device length. The ON/OFF normalized optical contrast was increased from 23% to 39% when the VO₂-on-Si region length was increased from 4 to $12 \mu\text{m}$. The inset of Figure 3d shows the computed mode profile (transverse-electric (TE) polarized) for the hybrid VO₂-Si waveguide section.

A minimum optical writing energy was determined using a single short laser pulse obtained from an optical intensity modulator (3 dB bandwidth of ~ 20 GHz). A continuous-wave laser operating at $1.5 \mu\text{m}$ was modulated by a single electrical voltage pulse from an arbitrary function generator. The writing optical pulse was generated by an external modulator coupled to a laser, and it had a pulse width of 500 ns and an extinction ratio >17 dB. The pulse width was chosen to be longer than the rise time of IMT that will be discussed later. The effective incident peak power launched into the VO₂-on-Si region was in the range of $150\text{--}450 \mu\text{W}$. The VO₂ wire was biased at 0.2 V less than the IMT voltage, and the change in the current was measured. To find the minimum optical power required for

writing the VO₂, the laser power was decreased until the IMT was no longer observed.

To simulate the fraction of light absorbed in the VO₂, we used the three-dimensional finite-difference time-domain method. The device structure sizes were based on the fabrication result and the complex refractive index of VO₂ insulator state $(n, k) = (3.13, 0.37)$ at a wavelength of $1.5 \mu\text{m}$ was adopted.³¹ As shown in the right y-axis of Figure 4a, the

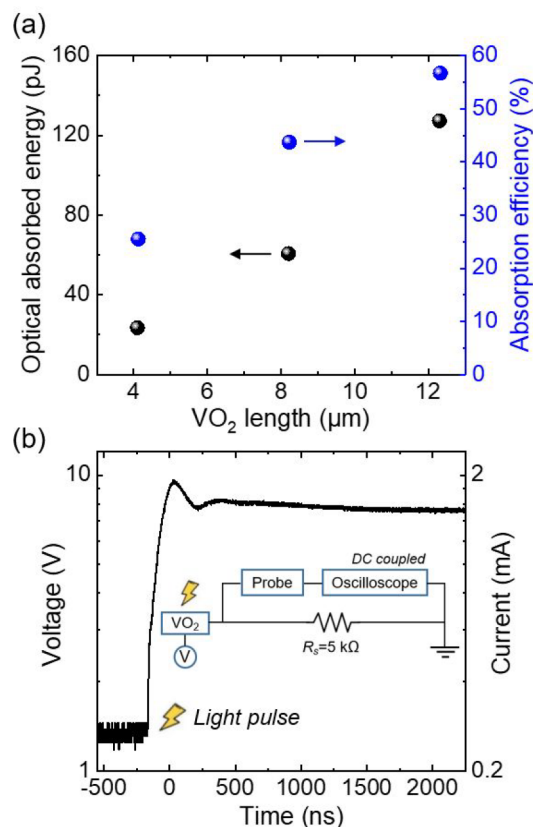


Figure 4. Optical memory characterization. (a) Measured minimum optical writing energy with the estimated light absorption efficiency in VO₂ plotted blue (right y-axis) for different VO₂ wire lengths. (b) Time trace of the voltage in a log scale across $R_s = 5 \text{ k}\Omega$ during the light-induced IMT showing a rise time of ~ 101 ns. The inset shows a circuit diagram of the electrical measurement setup.

absorption efficiency monotonically increases with the VO₂ length; for a $12 \mu\text{m}$ length, the absorption efficiency reaches $\sim 57\%$. Figure 4a plots the calculated absorbed optical energy for memory writing as a function of the VO₂ length. The absorbed optical energy was decreased as the VO₂ length was decreased, reaching a minimum energy of ~ 23.5 pJ with an absorption ratio of $\sim 25.5\%$ for the length of $4 \mu\text{m}$. The low absorption efficiency as well as low ON/OFF contrast was due to the low overlap between the VO₂ and the waveguide mode, as shown in the mode profile of the inset of Figure 3d. With further optimizations of the waveguide structure and coupling region in future work, a lower optical writing energy and a higher contrast in optical transmission can be expected.

To investigate the rise time of the IMT, we used the setup shown in the inset of Figure 4b; the voltage across R_s was recorded by a digital oscilloscope via a passive probe. The measurement setup without the VO₂ device had a $10\text{--}90\%$ rise time of 850 ps. Figure 4b shows that the voltage (and the

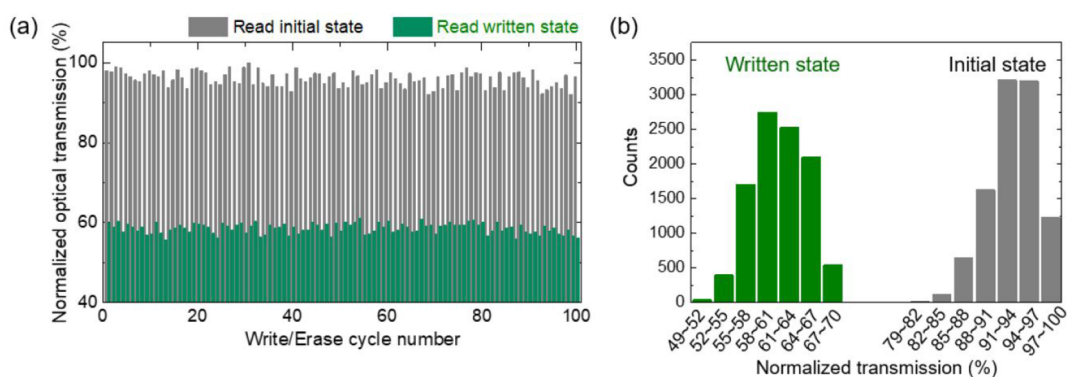


Figure 5. (a) Optical transmission readout for 100 repetitions of the write/erase cycle. A VO₂ device length of $\sim 12 \mu\text{m}$ was measured and ~ 150 ms-long optical pulse with an incident power of $\sim 820 \mu\text{W}$ was applied on the VO₂ wire biased at 9 V. (b) Distribution of the optical transmission for 10000 cycles (VO₂ devices length: $\sim 8 \mu\text{m}$). The voltage bias and incident optical power were ~ 8.5 V and $\sim 820 \mu\text{W}$, respectively.

inferred current, right axis) first abruptly increased as the VO₂ resistance drops through the IMT and then stabilized after a transient oscillation. The 10–90% rise time of the rising edge was found to be ~ 101 ns. According to simulations of an equivalent electrical circuit model of the setup, the intrinsic circuit 10–90% rise time should only be ~ 2 ns (see [Supporting Information](#) for details); thus, the observed rise time of ~ 101 ns was not limited by the circuit but was likely due to the time scale of the SPT (which is thermally limited). The measured reset time to return to the initial insulator state (MIT) was $\sim 3.1 \mu\text{s}$, much longer than the IMT time. The reset time was most likely limited by the thermal dissipation to reverse the SPT.^{13,14} By designing the sizes and the thermal environment of the devices, the rise and reset time could be reduced.

Figure 5a shows 100 changes in the optical transmission readout upon repeated writing/erasing. The transmission was highly reproducible with clear distinguishable transmission levels. To erase the memory, we turned off the voltage bias, so the VO₂ device temperature dropped below the phase transition temperature. The metal state was not sustained once the voltage bias was removed. The histogram in Figure 5b shows the distributions of the initial and written state normalized transmissions for 10000 cycles. The mean transmission (and the respective standard deviation) of the initial and written state was $\sim 93.2\%$ ($\sim 3.3\%$) and $\sim 61.2\%$ ($\sim 3.7\%$), respectively. The distributions for each state resulted from the fluctuations of the measurements. We successfully measured over 10000 cycles without observing an irreversible change and any writing error.

CONCLUSION

In summary, we have demonstrated a compact hybrid VO₂–Si optical memory. The memory used the bistable characteristics of VO₂ and required a voltage bias within the IMT hysteresis. The VO₂ material phase (insulator or metal) was read out in the optical transmission of a Si waveguide integrated with the memory. An optical readout with an ON/OFF contrast of $\sim 23\%$ was achieved with an optical writing energy of 23.5 pJ and a 10–90% rise time of ~ 100 ns for a $4 \mu\text{m}$ long memory cell. Because the resistance changes of the device could be read out electrically, backend optical-to-electronic conversion by a photodetector was not required. We confirmed that the written state was preserved for at least 200 h under a voltage bias and the device has good reproducibility over 10000 write/erase cycles. The performance of our photonic memory could be

improved by optimizing the design of the coupling region between the VO₂ and Si waveguide and by reducing the device size. Although the switching speed of the proposed VO₂ memory cell is similar to or better than the previously reported results for chalcogen-based phase change materials,^{5,12} the switching time of the IMT in VO₂ could be further reduced to pico- and femto-second time scales. One possible way could be to precisely adjust an excitation source to only trigger the electronic Mott transition to minimize the parasitic heat generation and the SPT. The VO₂ optical memory shown here is volatile, but future efforts will focus on realizing the nonvolatile VO₂ memory for being energy-efficient based on our previous report, which utilizes the narrow hysteresis of the first major transition between insulator state and oscillating state in current-biased VO₂ at room temperature,³² as well as on investigating architectures that combine the memory with computing functionality.^{25–27}

ASSOCIATED CONTENT

Supporting Information

The Supporting Information is available free of charge at <https://pubs.acs.org/doi/10.1021/acsphotonics.1c01410>.

Simulation of an equivalent electrical circuit model of the setup (PDF)

AUTHOR INFORMATION

Corresponding Author

Youngho Jung – Max Planck Institute of Microstructure Physics, Halle 06120, Germany; orcid.org/0000-0001-8627-5168; Email: youngho.jung@mpi-halle.mpg.de

Authors

Hyeon Han – Max Planck Institute of Microstructure Physics, Halle 06120, Germany; orcid.org/0000-0002-2973-5225

Ankita Sharma – Max Planck Institute of Microstructure Physics, Halle 06120, Germany; Department of Electrical and Computer Engineering, University of Toronto, Toronto, Ontario M5S 3G4, Canada

Junho Jeong – Department of Electrical and Computer Engineering, University of Toronto, Toronto, Ontario M5S 3G4, Canada; orcid.org/0000-0002-7179-4384

Stuart S. P. Parkin – Max Planck Institute of Microstructure Physics, Halle 06120, Germany

Joyce K. S. Poon – Max Planck Institute of Microstructure Physics, Halle 06120, Germany; Department of Electrical and Computer Engineering, University of Toronto, Toronto, Ontario M5S 3G4, Canada

Complete contact information is available at:

<https://pubs.acs.org/10.1021/acsphotonics.1c01410>

Author Contributions

[‡]These authors contributed equally to this work.

Funding

Open access funded by Max Planck Society.

Notes

The authors declare no competing financial interest.

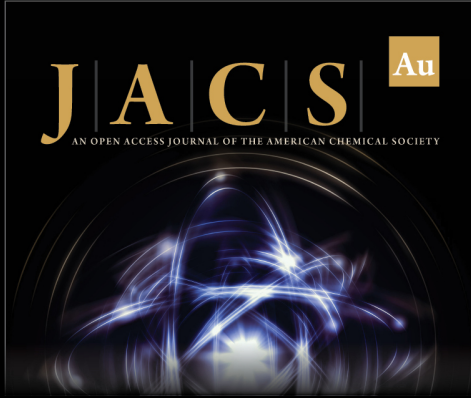
ACKNOWLEDGMENTS

The authors would like to thank Dr. Frank Heyroth for the cross-sectional SEM image.


REFERENCES

- (1) Alexoudi, T.; Kanellos, G. T.; Pleros, N. Optical RAM and integrated optical memories: a survey. *Light Sci. Appl.* **2020**, *9* (1), 1–16.
- (2) Sakaguchi, J.; Katayama, T.; Kawaguchi, H. High switching-speed operation of optical memory based on polarization bistable vertical-cavity surface-emitting laser. *IEEE J. Quantum Electron.* **2010**, *46* (11), 1526–1534.
- (3) Liu, L.; Kumar, R.; Huybrechts, K.; Spuesens, T.; Roelkens, G.; Geluk, E.-J.; de Vries, T.; Regreny, P.; Van Thourhout, D.; Baets, R.; Morthier, G. An ultra-small, low-power, all-optical flip-flop memory on a silicon chip. *Nat. Photonics* **2010**, *4* (3), 182–187.
- (4) Fitsios, D.; Alexoudi, T.; Bazin, A.; Monnier, P.; Raj, R.; Miliou, A.; Kanellos, G. T.; Pleros, N.; Raineri, F. Ultra-compact III–V-on-Si photonic crystal memory for flip-flop operation at 5 Gb/s. *Opt. Express* **2016**, *24* (4), 4270–4277.
- (5) Ríos, C.; Stegmaier, M.; Hosseini, P.; Wang, D.; Scherer, T.; Wright, C. D.; Bhaskaran, H.; Pernice, W. H. P. Integrated all-photonic non-volatile multi-level memory. *Nat. Photonics* **2015**, *9* (11), 725.
- (6) Zheng, J.; Khanolkar, A.; Xu, P.; Colburn, S.; Deshmukh, S.; Myers, J.; Frantz, J.; Pop, E.; Hendrickson, J.; Doylend, J.; Boechler, N.; Majumdar, A. GST-on-silicon hybrid nanophotonic integrated circuits: a non-volatile quasi-continuously reprogrammable platform. *Opt. Mater. Express* **2018**, *8* (6), 1551–1561.
- (7) Feldmann, J.; Youngblood, N.; Wright, C. D.; Bhaskaran, H.; Pernice, W. H. P. All-optical spiking neurosynaptic networks with self-learning capabilities. *Nature* **2019**, *569* (7755), 208.
- (8) Zhang, Y.; Chou, J. B.; Li, J.; Li, H.; Du, Q.; Yadav, A.; Zhou, S.; Shalaginov, M. Y.; Fang, Z.; Zhong, H.; et al. Broadband transparent optical phase change materials for high-performance nonvolatile photonics. *Nat. Commun.* **2019**, *10* (1), 1–9.
- (9) Feldmann, J.; Youngblood, N.; Karpov, M.; Gehring, H.; Li, X.; Stappers, M.; Le Gallo, M.; Fu, X.; Lukashchuk, A.; Raja, A. S.; et al. Parallel convolutional processing using an integrated photonic tensor core. *Nature* **2021**, *589* (7840), 52–58.
- (10) Delaney, M.; Zeimpekis, I.; Lawson, D.; Hewak, D. W.; Muskens, O. L. A new family of ultralow loss reversible phase-change materials for photonic integrated circuits: Sb₂S₃ and Sb₂Se₃. *Adv. Funct. Mater.* **2020**, *30* (36), 2002447.
- (11) Delaney, M.; Zeimpekis, I.; Du, H.; Yan, X.; Banakar, M.; Thomson, D. J.; Hewak, D. W.; Muskens, O. L. Nonvolatile programmable silicon photonics using an ultralow-loss Sb₂Se₃ phase change material. *Sci. Adv.* **2021**, *7* (25), eabg3500.
- (12) Fang, Z.; Zheng, J.; Saxena, A.; Whitehead, J.; Chen, Y.; Majumdar, A. Non-volatile reconfigurable integrated photonics enabled by broadband low-loss phase change material. *Adv. Opt. Mater.* **2021**, *9* (9), 2002049.
- (13) Shao, Z.; Cao, X.; Luo, H.; Jin, P. Recent progress in the phase-transition mechanism and modulation of vanadium dioxide materials. *NPG Asia Mater.* **2018**, *10* (7), 581–605.
- (14) Cuffey, S.; John, J.; Zhang, Z.; Parra, J.; Sun, J.; Orobtcouk, R.; Ramanathan, S.; Sanchis, P. VO₂ nanophotonics. *APL Photonics* **2020**, *5* (11), 110901.
- (15) Jeong, J.; Aetukuri, N.; Graf, T.; Schladt, T. D.; Samant, M. G.; Parkin, S. S. Suppression of metal-insulator transition in VO₂ by electric field-induced oxygen vacancy formation. *Science* **2013**, *339* (6126), 1402–1405.
- (16) Driscoll, T.; Kim, H.-T.; Chae, B.-G.; Di Ventra, M.; Basov, D. N. Phase-transition driven memristive system. *Appl. Phys. Lett.* **2009**, *95* (4), 043503.
- (17) Pellegrino, L.; Manca, N.; Kanki, T.; Tanaka, H.; Biasotti, M.; Bellingeri, E.; Siri, A. S.; Marré, D. Multistate memory devices based on free-standing VO₂/TiO₂ microstructures driven by Joule self-heating. *Adv. Mater.* **2012**, *24* (21), 2929–2934.
- (18) Bae, S. H.; Lee, S.; Koo, H.; Lin, L.; Jo, B. H.; Park, C.; Wang, Z. L. The memristive properties of a single VO₂ nanowire with switching controlled by self-heating. *Adv. Mater.* **2013**, *25* (36), 5098–5103.
- (19) Briggs, R. M.; Pryce, I. M.; Atwater, H. A. Compact silicon photonic waveguide modulator based on the vanadium dioxide metal-insulator phase transition. *Opt. Express* **2010**, *18* (11), 11192–11201.
- (20) Ryckman, J. D.; Hallman, K. A.; Marvel, R. E.; Haglund, R. F.; Weiss, S. M. Ultra-compact silicon photonic devices reconfigured by an optically induced semiconductor-to-metal transition. *Opt. Express* **2013**, *21* (9), 10753–10763.
- (21) Joushaghani, A.; Jeong, J.; Paradis, S.; Alain, D.; Aitchison, J. S.; Poon, J. K. S. Wavelength-size hybrid Si-VO₂ waveguide electro-absorption optical switches and photodetectors. *Opt. Express* **2015**, *23* (3), 3657–3668.
- (22) Miller, K. J.; Haglund, R. F.; Weiss, S. M. Optical phase change materials in integrated silicon photonic devices. *Opt. Mater. Express* **2018**, *8* (8), 2415–2429.
- (23) Shibuya, K.; Atsumi, Y.; Yoshida, T.; Sakakibara, Y.; Mori, M.; Sawa, A. Silicon waveguide optical modulator driven by metal-insulator transition of vanadium dioxide cladding layer. *Opt. Express* **2019**, *27* (4), 4147–4156.
- (24) Wong, H. M. K.; Yan, Z.; Hallman, K. A.; Marvel, R. E.; Prasankumar, R. P.; Haglund, R. F.; Helmy, A. S. Broadband, integrated, micron-scale, all-optical Si₃N₄/VO₂ modulators with pJ switching energy. *ACS Photonics* **2019**, *6* (11), 2734–2740.
- (25) Yi, W.; Tsang, K. K.; Lam, S. K.; Bai, X.; Crowell, J. A.; Flores, E. A. Biological plausibility and stochasticity in scalable VO₂ active memristor neurons. *Nat. Commun.* **2018**, *9* (1), 1–10.
- (26) Parihar, A.; Shukla, N.; Datta, S.; Raychowdhury, A. Synchronization of pairwise-coupled, identical, relaxation oscillators based on metal-insulator phase transition devices: A model study. *J. Appl. Phys.* **2015**, *117* (5), 054902.
- (27) Corti, E.; Khanna, A.; Niang, K.; Robertson, J.; Moselund, K. E.; Gotsmann, B.; Datta, S.; Karg, S. Time-delay encoded image recognition in a network of resistively coupled VO₂ on Si oscillators. *IEEE Electron Device Lett.* **2020**, *41* (4), 629–632.
- (28) Crunteanu, A.; Givernaud, J.; Leroy, J.; Mardivirin, D.; Champeaux, C.; Orlianges, J.-C.; Catherinot, A.; Blondy, P. Voltage- and current-activated metal-insulator transition in VO₂-based electrical switches: a lifetime operation analysis. *Sci. Technol. Adv. Mater.* **2010**, *11* (6), 065002.
- (29) Choi, S.; Word, M. J.; Kumar, V.; Adesida, I. Comparative study of thermally cured and electron-beam-exposed hydrogen silsesquioxane resists. *J. Vac. Sci. Technol. B* **2008**, *26* (5), 1654–1659.
- (30) Zhou, X.; Zhao, L.; Zhen, W.; Lin, Y.; Wang, C.; Pan, T.; Li, L.; Du, G.; Lu, L.; Cao, X.; Li, D. Phase-transition-induced VO₂ thin film IR photodetector and threshold switching selector for optical neural network applications. *Adv. Electron. Mater.* **2021**, *7* (5), 2001254.
- (31) Kim, M.; Jeong, J.; Poon, J. K. S.; Eleftheriades, G. V. Vanadium-dioxide-assisted digital optical metasurfaces for dynamic wavefront engineering. *J. Opt. Soc. Am. B* **2016**, *33* (5), 980–988.


(32) Jung, Y.; Jeong, J.; Qu, Z.; Cui, B.; Khanda, A.; Parkin, S. S.; Poon, J. K. Observation of optically addressable nonvolatile memory in VO₂ at room temperature. *Adv. Electron. Mater.* **2021**, *7* (8), 2001142.




JACS Au
AN OPEN ACCESS JOURNAL OF THE AMERICAN CHEMICAL SOCIETY



Editor-in-Chief
Prof. Christopher W. Jones
Georgia Institute of Technology, USA

Open for Submissions 

pubs.acs.org/jacsau  ACS Publications
Most Trusted. Most Cited. Most Read.